Nuclear Science and Techniques (2024) 35:70
https://doi.org/10.1007/s41365-024-01431-3

Design of weak current measurement system and research on temperature impact

Chu-Xiang Zhao[1] · San-Gang Li[1,2] · Rong-Rong Su[1] · Li Yang[3] · Ming-Zhe Liu[1,2] · Qing-Yue Xue[1] · Shan Liao[1] · Zhi Zhou[1] · Qing-Shan Tan[1] · Xian-Guo Tuo[4] · Yi Cheng[1]

Received: 18 October 2023 / Revised: 20 November 2023 / Accepted: 25 November 2023 / Published online: 9 May 2024
© The Author(s), under exclusive licence to China Science Publishing & Media Ltd. (Science Press), Shanghai Institute of Applied Physics, the Chinese Academy of Sciences, Chinese Nuclear Society 2024

Abstract

A dedicated weak current measurement system was designed to measure the weak currents generated by the neutron ionization chamber. This system incorporates a second-order low-pass filter circuit and the Kalman filtering algorithm to effectively filter out noise and minimize interference in the measurement results. Testing conducted under normal temperature conditions has demonstrated the system's high precision performance. However, it was observed that temperature variations can affect the measurement performance. Data were collected across temperatures ranging from −20 to 70 °C, and a temperature correction model was established through linear regression fitting to address this issue. The feasibility of the temperature correction model was confirmed at temperatures of −5 and 40 °C, where relative errors remained below 0.1% after applying the temperature correction. The research indicates that the designed measurement system exhibits excellent temperature adaptability and high precision, making it particularly suitable for measuring weak currents.

Keywords Weak current measurement system · Neutron ionization chamber · Kalman filter algorithm · Temperature correction model

1 Introduction

In the context of striving for carbon neutrality and carbon peaking, the advancement of clean and efficient nuclear energy has emerged as a strategic imperative [1–6]. Within the realm of nuclear energy, real-time monitoring of reactor power plays a crucial role in providing insights into the operational status of the reactor [7–12]. One common instrument employed for this purpose is the neutron ionization chamber [13], which enables the reflection of reactor powers that are inherently linked to the aforementioned flux rates. Therefore, precise measurement of the output current of the neutron ionization chamber assumes paramount importance.

The output current amplitude of the neutron ionization chamber is exceptionally low, falling under the category of weak electrical currents [14–16]. Typically, these current signals range from 10^{-4} to 10^{-11}A [17, 18]. Given the delicate nature of weak current measurements, even minor interferences can introduce undesirable fluctuations, subsequently leading to inaccuracies in the resulting measurements [19]. Such interferences manifest as electrical, electromagnetic, and thermoelectric noise arising from

This work was supported by the Youth Science Foundation of Sichuan Province (Nos. 2022NSFSC1230 and 2022NSFSC1231), the Science and Technology Innovation Seedling Project of Sichuan Province (No. MZGC20230080), the General project of the National Natural Science Foundation of China (No. 12075039), and the Key project of the National Natural Science Foundation of China (No. U19A2086).

✉ San-Gang Li
lisangang@cdut.edu.cn

[1] College of Nuclear Technology and Automation Engineering, Chengdu University of Technology, 1#, Dongsanlu, Erxianqiao, Chengdu 610059, China

[2] Applied Nuclear Technology in Geosciences Key Laboratory of Sichuan Province , Chengdu University of Technology, 1#, Dongsanlu, Erxianqiao, Chengdu 610059, China

[3] University of Science and Technology of China, Hefei 230026, China

[4] School of Physics and Electronic Engineering, Sichuan University of Science and Engineering, Zigong 643000, China

unpredictable temperature variations [20–22]. Factors such as the choice of printed circuit board (PCB) material and circuit wiring methods contribute to the problem of leakage currents, which further compromises the measurement accuracy of the overall system [23–25].

Simple amplification of input weak current signals cannot obtain accurate signal values owing to the presence of noise. Usually, they are converted into alternative values and subsequently amplified [26, 27]. Two commonly employed methods for measuring weak currents are the current-to-frequency conversion (IFC) and the current-to-voltage conversion (IVC) [26–30]. While effective, the measurement system based on IFC presents a complex structure and intricate circuit debugging, rendering it unsuitable for real-time acquisition and high-speed signal conversion [31]. IVC emerges as the prevalent design approach for weak current measurements. It encompasses two specific implementation methods: capacitance integration and trans-impedance amplification [21]. Although suitable for measuring the average value of unstable currents, the capacitance integration method falls short when faced with rapid changes or continuous measurements [32]. The trans-impedance amplification method offers a real-time measurement approach by converting current into voltage through an operational amplifier and feedback resistance. However, it does require a large feedback resistance, making it susceptible to temperature variations [33].

Scholars have conducted some research with various achievements in the realm of weak current measurement. Guo et al. employed the trans-impedance amplification method to design a weak current measurement system capable of measuring currents ranging from μA to pA [26]. While they acknowledged the impact of temperature on the measurement system, they did not conduct performance testing. Hao et al. utilized the dual switching capacitance integration method to design a weak current measurement circuit. By testing the circuit at 15 °C, they achieved a measurement relative error below 4% at the nA level and 0.5% at the μA level [24]. Wang et al. based their study on the high-resistance IVC method and designed a pA-level current measurement circuit. They tested the circuit at normal temperature (25 °C) and found that the maximum measurement error was 1.5% [25]. Zhao et al. designed a weak current measurement circuit capable of measuring currents ranging from nA to pA based on the IFC method. They utilized the Keithley 6430 as a standard current source during the experimental test at normal temperature. The results indicated relative errors within 3% in the effective range and 1% in the medium or high range [34]. In summary, while these articles shed light on the influence of temperature on measurement results, studies on mitigating this effect are limited.

This study presents a high-precision weak current measurement system equipped with temperature correction to address the challenges posed by the weak current output signal of the neutron ionization chamber. Primarily, the ADA4530-1 operational amplifier is utilized as a trans-impedance amplifier in the preamplifier circuit design. Several measures are taken in the hardware circuit design to minimize the impact of interference noise on the weak current signal. Furthermore, the host computer software is developed using the integrated development environment of Visual Studio + Qt. In the software section, the Kalman filtering algorithm was added to filter the weak current signal, thereby enhancing the stability and accuracy of the system. The performance of this system is then tested and analyzed at a normal temperature. Finally, we explore the influence of temperature drift on the measurement accuracy of the system and propose a temperature correction model to mitigate its effects.

2 System design

In this study, a weak current measurement system was designed for a neutron ionization chamber. The system comprises two main components: a hardware system and a host computer control system, as illustrated in Fig. 1. The weak currents are initially amplified and converted into negative analog voltage signals using the IVC preamplifier circuit. The amplification factor is controlled by the range-switching circuit. Subsequently, the voltage signals undergo filtering via a second-order low-pass filter circuit. The negative signals are transformed into positive signals via an inverse amplifier circuit, thereby facilitating further processing. The processed signals are then transmitted to an analog-to-digital conversion (ADC) circuit, where the analog voltage signals

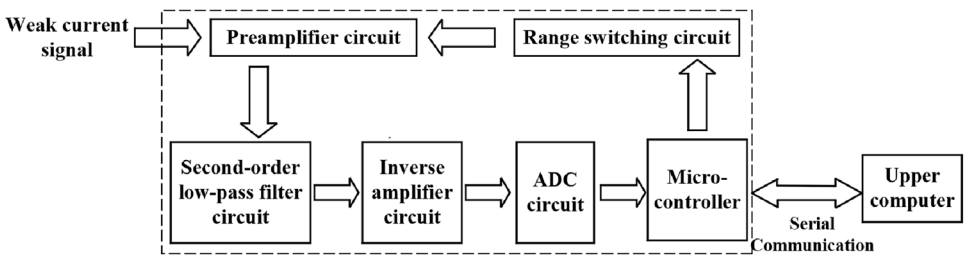

Fig. 1 Structural diagram of the weak current measurement system

are converted into digital voltage signals. These digital voltage signals are subsequently transmitted to a microcontroller, which establishes data transmission with the host computer system through serial communication. Finally, in the host computer control system, comprehensive functionalities such as data exchange between the hardware system and the host computer, data processing, real-time display, and storage of collected data are realized.

2.1 Design of hardware system

To capture the weak current signal emitted from the neutron ionization chamber, a preamplifier circuit utilizing ADA4530-1 was devised [34]. This circuit comprises IVC preamplifier, second-order low-pass filter, and inverse amplifier circuits, among others. The schematic diagram of the IVC method can be observed in Fig. 2.

The output voltage of the IVC preamplifier circuit in the ideal state is:

$$V_0 = -R_f I_{in} \tag{1}$$

where V_0 represents an output voltage, R_f represents a feedback resistance value, and I_{in} represents an input current of the IVC amplification circuit.

As shown in Eq. (1), the feedback resistance value determines the amplification factor of weak currents. It is imperative to carefully select this resistance value, avoiding either too high or too low values. The rationale is that the feedback resistance value must match the input range of the backend ADC to achieve higher resolution. In practice, choosing the feedback resistance value depends on the magnitude of the current being measured. Low currents require a large resistance, while higher currents require a smaller resistance. This study accomplished this goal by utilizing resistance values of 500 MΩ and 50 KΩ. The currents are divided into two gears based on these feedback resistance values, namely 10 nA gear (500 MΩ) and 0.1 mA gear (50 KΩ). A gear-switching

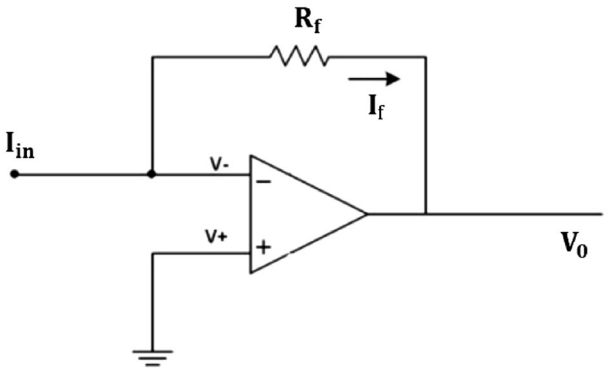

Fig. 2 Schematic diagram of the IVC method

circuit was designed to achieve automatic resistance switching. This circuit enabled the microcontroller to control the on/off state of the optocoupler TLP521 by manipulating the corresponding pin's high and low-level outputs, thereby realizing the on/off of the relay for switching gears.

Furthermore, the performance of operational amplifiers can be significantly influenced by various manufacturing processes and material characteristics. These factors can introduce deviations in the output voltage of the IVC amplification circuits. The actual output voltage of this circuit should be:

$$V_0 = -R_f I_{in} + R_f I_B + (V_{0s} - V_0/A), \tag{2}$$

where A represents the open-loop gain of operational amplifiers, I_B represents the input bias current, and V_{0s} represents the input offset voltage.

According to Eq. (1) and Eq. (2), if the input bias current and input offset voltage are small and the open-loop gain is large, then the error between the actual output voltage and the ideal situation is relatively small. Therefore, to enhance the accuracy of the measurement system, the operational amplifier ADA4530-1 is employed as a trans-impedance amplifier within the preamplifier circuit, owing to its distinct advantages. These include its ultra-low input bias current, which is much smaller than the measured current, its lower offset voltage, and its high open-loop gain and CMRR, which can minimize the influence of error caused by input voltage drop. Furthermore, the ADA4530-1 also incorporates a built-in guard ring buffer that isolates the input pins, thus preventing interference due to current noise leakage from the PCB board.

The IVC preamplifier circuit, as illustrated in Fig. 3a, converts weak current signals into voltage signals and subsequently amplifies them. The second-order low-pass filter circuit is employed to mitigate the detrimental effects of high-frequency noise on the measurement system, as depicted in Fig. 3b. This filter circuit effectively eliminates high-frequency noise from the amplified voltage signal outputted by the amplifier circuit. The inverse amplifier circuit ensures that the voltage value transmitted to the ADC circuit is positive, and its design is shown in Fig. 3c.

The ADC circuit converts the output voltage signal from the inverter amplifier circuit into a digital signal representation. The stability and linearity performance of the ADC directly impacts the accuracy of the overall measurement system. In this circuit, AD7172-2 with 24-bit high precision manufactured by Analog Devices, Inc. (ADI), is employed. It can sample the output voltage at a high sampling rate of 100 MHz and convert an analog voltage signal into a digital signal, as shown in Fig. 3d.

When measuring weak current signals, various minor interferences can introduce errors. Consequently, this study

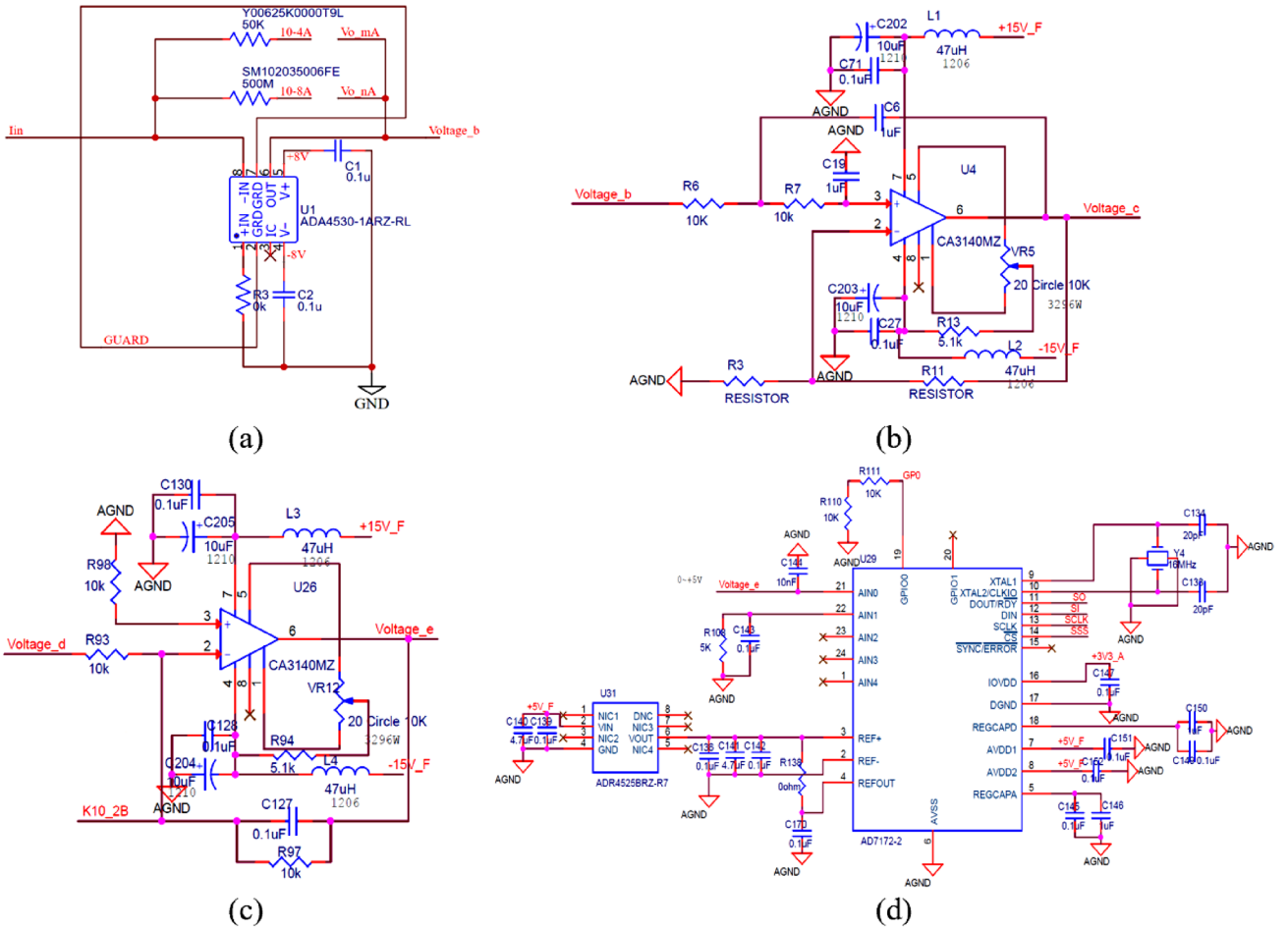

Fig. 3 Hardware circuit diagram. IVC preamplifier circuit **a**, Second-order low-pass filter circuit **b**, Inverter amplifier circuit **c**, and ADC circuit **d**

implements several measures for the hardware circuit to improve the anti-interference performance of the measurement system during the measurement of weak current signals. Firstly, high-quality PCB with excellent insulation properties is employed to minimize the impact of leakage current. Secondly, a metallic aluminum conductor is utilized to enclose the entire measurement system, creating a Faraday cage that effectively shields electromagnetic interference. Lastly, a triaxial cable with strong anti-interference capabilities is used as the signal input line, with an added insulation layer and shielding braid outside the cable to reduce electromagnetic interference on the weak current signal further.

2.2 Design of host computer software system

The host computer software in this system was developed utilizing the integrated development environment (IDE) of Visual Studio and Qt, serving as the pivotal controller for the entire system. Firstly, the main operation page configures the serial port parameters to initiate intercommunication between the host computer and the hardware system. Upon establishing a successful connection, the hardware system executes corresponding operations based on the parsed command packet sent by the host computer. Finally, the hardware system transmits the measured data to the host computer via the serial port. The host computer software analyzes and processes the data packets and displays a 2D weak current signal waveform diagram.

During the weak current measurement process, the presence of interferences arising from experimental environments and leakage currents can introduce noise bursts into the measured signals. These interferences result in fluctuations in the measurement outcomes. The Kalman filtering algorithm can estimate the state of a dynamic system from a series of data with measurement noise when the measurement variance is known [35, 36]. The Kalman filtering algorithm was incorporated into the host computer software program to further enhance the accuracy of the measurement results. This facilitated the filtration of the measured

data, thereby effectively enhancing the overall stability of the system.

3 Analysis and discussion

3.1 Test in normal temperature

During the testing process, the weak current measurement system was placed inside the Giant Force constant temperature and low humidity test chamber, with the relative humidity set at 10% and the temperature set at 25 °C, as illustrated in Fig. 4. The Keithley 6430 source meter was used to generate standard weak currents [37]. The output current waveforms (250 measurement points) of the measurement system are depicted in Fig. 5. It can be observed from Fig. 5 that the waveform data exhibited slight fluctuations around their respective average measurement currents (presented in Table 1) for both the 10 nA and 0.1 mA gears. Moreover, these average values closely approximated the respective standard input currents.

To further illustrate the above conclusion, the relative errors and relative standard deviations (RSDs) were used to quantitatively evaluate this waveform data [38, 39]. The relative errors between the input standard currents and average measurement currents were employed to represent the accuracy; the RSDs between sample point values and their average measurement currents were employed to represent the precision; and the relative errors and RSDs for the waveform data were obtained, which are also shown in Table 1.

Table 1 shows that the measurement system had very small relative errors and RSDs in both the 10 nA and 0.1 mA gears. For example, their relative errors were maintained less than or equal to 0.086% in 10 nA gear and 0.124% in 0.1 mA gear; when the standard input currents were 1 nA and 0.07 mA, their relative errors reached an astonishing 0.010% and 0.006%, and their RSDs were only 0.0106% and 0.0002%, respectively. These qualitative and quantitative results demonstrate that this system has high accuracy and precision at normal temperatures.

Note: due to the minimal errors, a significant number of decimal places are retained. Five bits in the 10 nA gear and seven bits in the 0.1 mA gear are used to represent the decimal places of the current measurement.

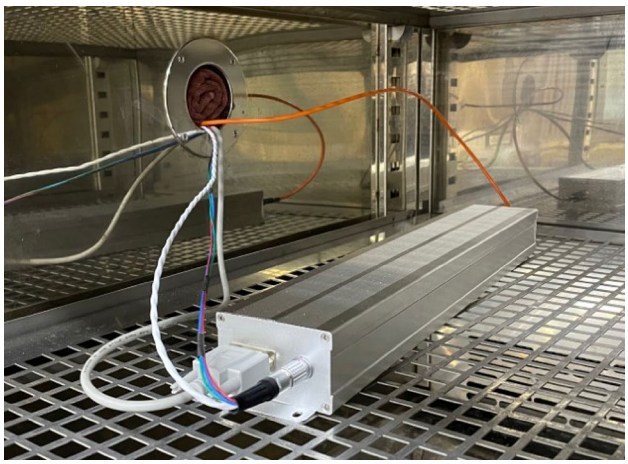

Fig. 4 (Color online) Measurement system in the constant temperature and humidity test chamber

3.2 Test in different temperatures

In order to ascertain the performance of a current measurement system at various ambient temperatures, we meticulously conducted a series of temperature experiments within a controlled test chamber. Consistently maintaining each temperature, we meticulously recorded the continuous measurements of the system while subjecting it to distinct standard input currents. When the measurement system was in the 10 nA gear, these standard input current values included 0.5 nA, 1 nA, 4 nA, and 7 nA. Similarly, when the measurement system was in the 0.1mA gear, our chosen standard current values encompassed 0.01 mA, 0.04 mA, 0.07 mA, and 0.1 mA. Subsequently, we proceeded to alter the temperature and repeated these steps. Our experimental endeavors encompassed a broad spectrum of temperatures, encompassing −20 °C, −10 °C, 0 °C, 15 °C, 35 °C, 45 °C, 55 °C, and 70 °C.

We averaged some measurement results attained from the distinct input standard current values and presented the averaged results in Tables 2 and 3. Notably, the data at 25 °C were acquired from a previous experiment conducted at normal temperature conditions, contributing valuable reference points for our analysis. Also, the relative errors between the averaged measurement currents and standard input currents were computed, as shown in Tables 2 and 3.

Tables 2 and 3 show that the measured values gradually decrease as the temperatures increase under the same input currents. This indicates that temperature has an impact on the measurement system. In Table 3, when the standard input current is set to 0.1 mA, and the ambient temperature falls below 25 °C, an intriguing phenomenon arises within the measurement system. The system's output remains stable, unwavering at 0.1 mA. The following rationale can elucidate this occurrence: the value of 0.1 mA at the normal temperature corresponds to the maximum measurement capacity of the ADC. Consequently, when the ambient temperature descends below 25 °C, the output value of the ADC corresponding to the 10 mA input has already reached the pinnacle of its full-scale measurement capability. As a result, the current value displayed on the host computer remains unaltered, in a state of resolute constancy.

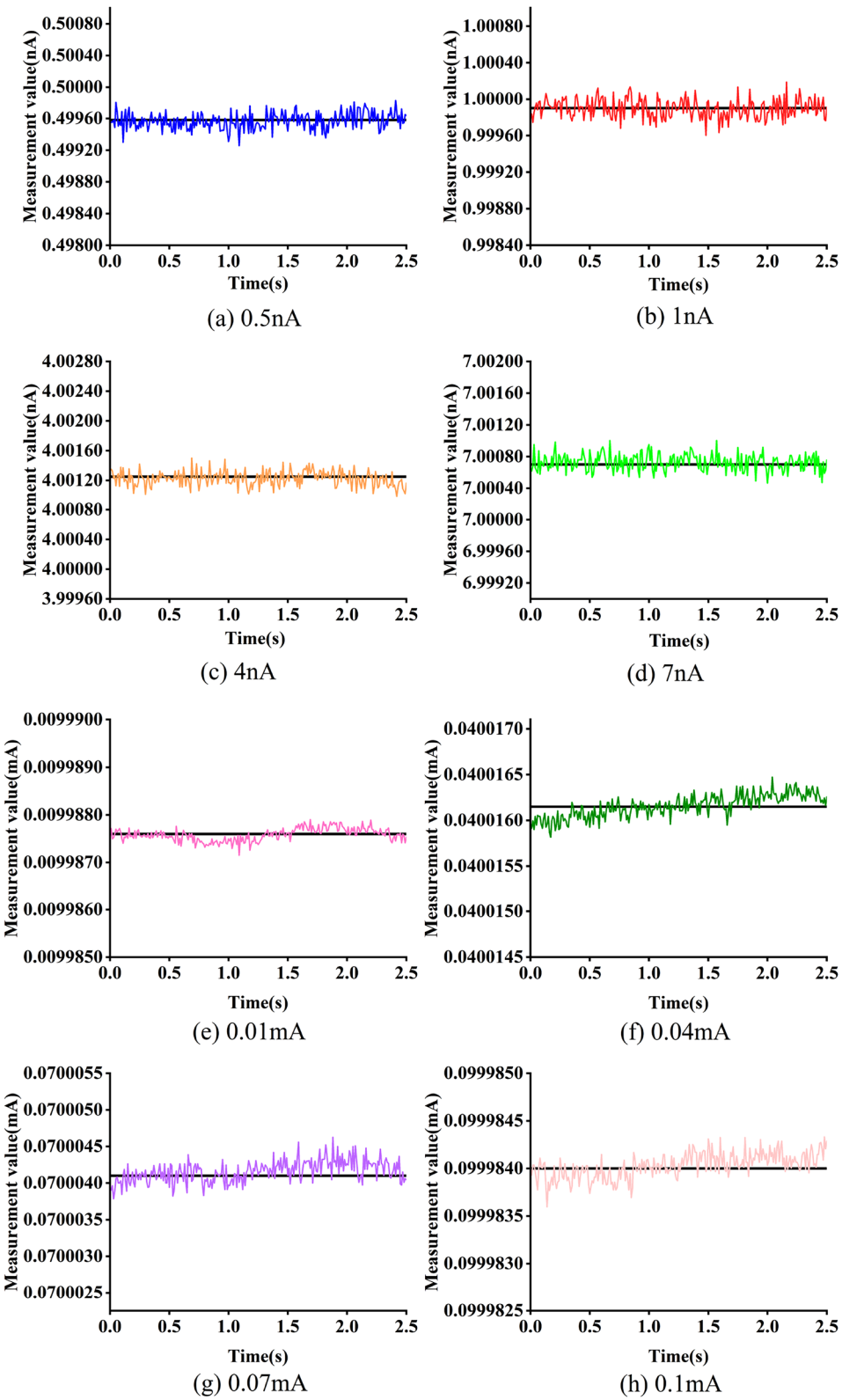

Fig. 5 (Color online) Measurement waveforms in 10 nA and 0.1 mA gears at normal temperature

Table 1 Measurement results of the system in the 10 nA gear

Standard current	Actual average measurement current	Relative error (%)	RSD (%)
0.5 nA	0.49957 nA	0.086	0.0207
1 nA	0.99990 nA	0.010	0.0106
4 nA	4.00123 nA	0.030	0.0025
7 nA	7.00072 nA	0.010	0.0015
0.01 mA	0.0099876 mA	0.124	0.0013
0.04 mA	0.0400162 mA	0.040	0.0003
0.07 mA	0.0700042 mA	0.006	0.0002
0.1 mA	0.0999840 mA	0.016	0.0001

Additionally, the relative errors are less than or equal to 0.484% in the Table 2 and 0.388% in the Table 3.

From Tables 2 and 3, it can be seen that the influence of temperature on the 10 nA gear is greater than that on the 0.1 mA gear, so the measurement results in the 10 nA gear should be corrected more than in the 0.1 mA gear; in the same standard input currents, using 25 °C as the dividing point, the rate of change of the relative error differs on both sides. For example, in the 10 nA gear, the relative error gradually decreases with increasing temperatures, reaching its minimum at 25 °C. Subsequently, as the temperature rises again, the relative error gradually increases. A similar situation also occurs in the 0.1 mA gear, except for 0.01 mA. This indicates that temperature significantly impacts the accuracy of our system, and it is necessary to correct the influence of temperature. Furthermore, under identical temperature conditions, in addition to normal temperature conditions, distinct input standard current values yield varying degrees of relative error when subjected to measurement. This revelation implies an intrinsic correlation between the input current and the resultant relative error.

In addition, the possible reasons for the absence of this phenomenon in 0.01 mA data are the comprehensive results of noise interference and temperature influence. The noise interference of the measurement system cannot be completely eliminated. In the same gear, the lower the

Table 2 Measurement results of the system in the 10 nA gear at different temperatures

T (°C)	0.5 nA		1 nA		4 nA		7 nA	
	Measurement current	Relative error (%)	Measurement current	Relative error (%)	Measurement current	Relative error (%)	Measurement current	Relative error (%)
−20	0.50184	0.368	1.00419	0.419	4.01680	0.420	7.02785	0.398
−10	0.50126	0.252	1.00293	0.293	4.01238	0.310	7.02021	0.289
0	0.50087	0.174	1.00212	0.212	4.00885	0.221	7.01378	0.197
15	0.49988	0.024	1.00061	0.061	4.00383	0.096	7.00527	0.075
25	0.49957	0.086	0.99993	0.007	4.00121	0.030	7.00071	0.010
35	0.49922	0.156	0.99924	0.076	3.99851	0.037	6.99604	0.057
45	0.49884	0.232	0.99857	0.143	3.99608	0.098	6.99186	0.116
55	0.49848	0.304	0.99791	0.209	3.99399	0.150	6.98827	0.168
70	0.49758	0.484	0.99668	0.332	3.99066	0.234	6.98270	0.247

Table 3 Measurement results of the system in the 0.1 mA gear at different temperatures

T (°C)	0.01 mA		0.04 mA		0.07 mA		0.1 mA	
	Measurement current	Relative error (%)	Measurement current	Relative error (%)	Measurement current	Relative error (%)	Measurement current	Relative error (%)
−20	0.0100025	0.025	0.0400891	0.223	0.0701279	0.183	0.1000000	0.000
−10	0.0100136	0.136	0.0400680	0.170	0.0700922	0.132	0.1000000	0.000
0	0.0099991	0.009	0.0400505	0.126	0.0700625	0.089	0.1000000	0.000
15	0.0099875	0.125	0.0400278	0.070	0.0700239	0.034	0.1000000	0.000
25	0.0099876	0.124	0.0400160	0.040	0.0700041	0.006	0.0999840	0.016
35	0.0100246	0.246	0.0400050	0.012	0.0699856	0.021	0.0999569	0.043
45	0.0099750	0.250	0.0399954	0.012	0.0699700	0.043	0.0999355	0.065
55	0.0099693	0.307	0.0399876	0.031	0.0699577	0.060	0.0999180	0.082
70	0.0099612	0.388	0.0399787	0.053	0.0699436	0.081	0.0998984	0.102

input current, the higher the proportion of noise interference in the current. This implies that more gears can be adopted to reduce the proportion of noise interference by making the ADC a high-bit output. The output current is also affected by temperature, leading to unstable output results.

3.3 Temperature correction model

We have established a mathematical relationship to accurately depict the influence of temperatures on the output current, as illustrated in Eq. (3). Notably, we observed that the slopes on either side of the normal temperature (25 °C) in Tables 2 and 3 were different. Therefore, the data were divided into two categories for obtaining parameter values in Eq. (3): temperatures below and above 25 °C.

In this study, we focused on analyzing the output current values of the 10 nA gear at temperatures below 25 °C. Initially, we conducted a linear regression analysis, examining the values of standard input current (x) and output current (y) at various temperatures (T). The detailed outcomes of this regression analysis can be found in Table 4.

$$y = K_T \times x + C \tag{3}$$

where K_T represents the slope value at temperature T and C represents an intercept.

Based on the data presented in Table 4, it was observed that all five linear fittings exhibited an R^2 value of 1, indicating a commendable level of fitting accuracy. This implied that the linear equations could effectively describe the relationship between the input standard current value and the corresponding output current value at the same temperature.

On the other hand, the intercept values in the five fitting equations were very small at different temperatures, having a very small impact on the output current values. This intercept part was disregarded in our model. When discussing the relationship between the system output current value and temperature, we only considered the relationship between the slope values of the linear equations and temperatures. Hence, the relationship between the two can be described by the following linear equation:

$$y = K_T \times x. \tag{4}$$

According to Eq. (4), we can use the relationship between K_T and y to correct measurement errors caused by temperatures. The corrected output currents can be represented by the slope values and output current values as follows:

$$Y = 1/K_T \times y, \tag{5}$$

where Y represents the corrected output current value.

When the same current value is input, the measurement system operates at different ambient temperatures and generates different K_T values. In order to correct the measurement error of the system at a certain temperature, it is necessary to find the relationship between the slope value and the temperature difference ΔT. The temperature difference ΔT and the five slope values in Table 4 were linearly fitted, where ΔT (Eq. (6)) represents the difference between the ambient temperature and 25 °C. The linear fitting equation was shown in Eq. (7).

$$\Delta T = T - 25 \tag{6}$$

$$K_T = -0.0000868 \times \Delta T + 0.9999 \tag{7}$$

Equation (7) shows a high degree of goodness of fit, indicating a strong linear relationship between the temperature difference (ΔT) and the slope values. This suggests that the slope values also increase or decrease consistently as the temperature difference increases or decreases. This linear relationship allows us to accurately correct the measurement error based on the ambient temperature difference. Thus, the temperature correction equation for the 10 nA gear at ambient temperature below 25 °C is:

$$Y_1 = y/(-0.0000868 \times (T - 25) + 0.9999). \tag{8}$$

Upon further examination, we expanded our analysis to encompass additional scenarios and unveiled a consistent linear relationship. Subsequently, by leveraging the practical measurements of test current values, we have successfully constructed models for the 10 nA gear at temperatures above 25 °C and for the 0.1 mA gear across both temperatures below and above 25 °C.

The temperature correction equation for the 10nA gear at ambient temperature above 25 °C is

$$Y_2 = y/(-0.000051 \times (T - 25) + 1.0000). \tag{9}$$

The temperature correction equation for the 0.1 mA gear at ambient temperature below 25 °C is

$$Y_3 = y/(-0.0000456 \times (T - 25) + 1.0000). \tag{10}$$

Table 4 Fitting parameter values for the 10 nA gear at temperatures below 25 °C

Temperature (°C)	Slope	Intercept	R^2
−20	1.0040	0.0002	1
−10	1.0029	0.0002	1
0	1.0020	0.0002	1
15	1.0008	−0.0002	1
25	1.0002	−0.0002	1

The temperature correction equation for the 0.1 mA gear at ambient temperature above 25 °C is

$$Y_4 = y/(-0.0000080 \times (T - 25) + 0.9997), \quad (11)$$

where Y_1, Y_2, Y_3, and Y_4 represent the corrected output current value.

3.4 Verification of correction model

Some standard weak currents ranging between −5 °C and 40 °C were measured to verify the temperature correction model. The relative errors of the measured data and corrected data are shown in Fig. 6.

We can intuitively deduce from Fig. 6a and c that at an ambient temperature of −5 °C, the relative error of the measured data remained remarkably below 0.25% in the 10nA gear and below 0.15% in the 0.1mA gear. Following the implementation of temperature correction, except for 0.1mA (it is at full scale with an error of 0 and does not need to be corrected in actual situations), as illustrated in Fig. 6c, the relative error was consistently maintained below 0.03% in the 10nA gear and below 0.066% in the 0.1mA gear. Consequently, through the utilization of the temperature correction model, the accuracy of the system's output has been greatly enhanced.

On the other hand, drawing from the valuable insights presented in Fig. 6b and d, we observe that at an ambient temperature of 40 °C, the relative error of the measured data remained consistently below 0.2% in the 10nA gear and below 0.1% in the 0.1 mA gear. Following the temperature correction procedure, the relative error was effectively maintained below 0.1% in the 10 nA gear and below 0.05% in the 0.1 mA gear.

In conclusion, the implementation of the temperature correction model can improve measurement accuracy by mitigating the influence of temperature fluctuations on the measurement system.

4 Conclusion

The weak current measurement system described in this study offers a novel approach to accurately measuring weak currents in a neutron ionization chamber. The filter circuit and the Kalman filter algorithm work together to effectively filter out noise and consequently enhance the overall accuracy of the measurements. However, temperatures have a negative impact on the accuracy of current measurements. The system described in this study includes a temperature correction model that effectively mitigates this impact, ensuring exceptional stability. This allows for accurate measurements even in varying temperature conditions. The test results of the system demonstrate remarkable precision. At the normal temperature, the system relative deviations reached an astonishing 0.010% in 1 nA and 0.006% in 0.07 mA, and their RSD were only 0.0106% and 0.0002%. Even in the −5 °C to 40 °C range, all relative deviations of the system were maintained below 0.1%. Additionally, some gears can be added appropriately to further increase accuracy. In

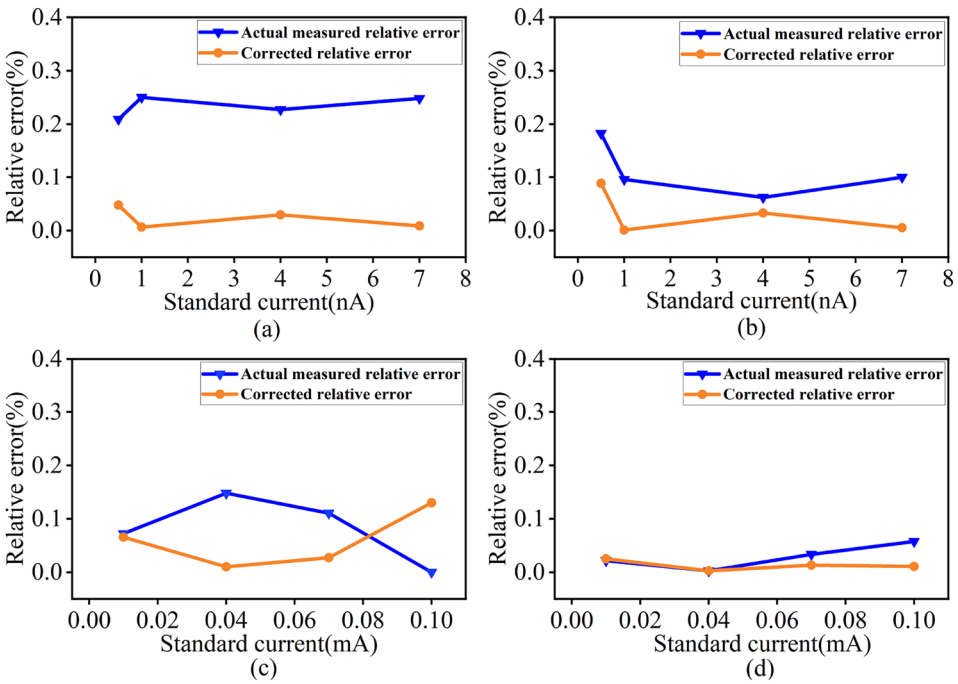

Fig. 6 (Color online) Relative error curves of the measured and corrected data. The results in the −5 °C and 40 °C range are shown in the first and second columns. The results for the 10 nA and 0.1 mA gears are shown in the first and second lines

summary, the weak current measurement system presented in this study offers high accuracy and stability and can accurately measure weak currents across a wide temperature spectrum. This system is not only limited to measuring fission current, as it can also be used in some scenarios where weak current needs to be measured, such as low-activity gas tritium measurement based on proportional counters. Further, this temperature correction model can be used to correct other instruments affected by temperatures.

Author Contributions All authors contributed to the study conception and design. Material preparation, data collection and analysis were performed by Chu-Xiang Zhao, San-Gang Li, Rong-Rong Su, and Li Yang. The first draft of the manuscript was written by Chu-Xiang Zhao and all authors commented on previous versions of the manuscript. All authors read and approved the final manuscript.

Data availability The data that support the findings of this study are openly available in Science Data Bank at https://cstr.cn/31253.11.sciencedb.16418 and https://www.doi.org/10.57760/sciencedb.16418.

Declarations

Conflict of interest The authors declare that they have no conflict of interest.

References

1. E.F.M, Ahmed, Dissertation, Sudan University of Science and Technology, 2011
2. C.A. Liu, X.M. Shi, The role of fusion-fission hybrid reactor in development of China nuclear energy resources. J. Strateg. Study CAE **26**, 24–28 (2011). https://doi.org/10.3969/j.issn.1009-1742.2011.03.004
3. X.X. Yang, B. Cai, Y.S. Xue, Review on optimization of nuclear power development: A cyber-physical-social system in energy perspective. J. Modern Power Syst. Clean Energy **10**, 547–561 (2022). https://doi.org/10.35833/MPCE.2021.000272
4. Z. Zhou, S.G. Li, Q.S. Tan et al., Optimization method of Hadamard coding plate in γ-ray computational ghost imaging. Nucl. Sci. Tech. **34**, 13 (2023). https://doi.org/10.1007/s41365-022-01164-1
5. H.R. Liu, M.Z. Liu, Y.L. Xiao et al., Discrimination of neutron and gamma ray using the ladder gradient method and analysis of filter adaptability. Nucl. Sci. Tech. **33**, 159 (2022). https://doi.org/10.1007/s41365-022-01136-5
6. Y.C. Yan, M.Z. Liu, X.Y. Li et al., Improved Cohen-Sutherland algorithm for TGS transmission imaging. Nucl. Sci. Tech. **34**, 98 (2023). https://doi.org/10.1007/s41365-023-01238-8
7. W. Xu, J. Li, H. Xie et al., Conceptual design and safety characteristics of a new multi-mission high flux research reactor. Nucl. Sci. Tech. **34**, 34 (2023). https://doi.org/10.1007/s41365-023-01191-6
8. W.P. Li, D.B. Yang, Design of reactor nuclear measurement systems in Ling'ao nuclear power station phase II. J. Nuclear Power Eng. **33**, 1–4 (2012). https://doi.org/10.3969/j.issn.0258-0926.2012.02.001
9. R.J. Zhu, X. Zhou, Z.H. Liu et al., High-precision and wide-range real-time neutron flux monitor system through multipoint linear calibration. Nucl. Sci. Tech. **31**, 94 (2020). https://doi.org/10.1007/s41365-020-00798-3
10. V.A. Varlachev, E.G. Emets, Y.C. Mu et al., Determining absolute value of thermal neutron flux density based on monocrystalline silicon in nuclear reactors. Nucl. Sci. Tech. **33**, 83 (2022). https://doi.org/10.1007/s41365-022-01077-z
11. V.T. Vo, V.K. Nguyen, N.D. Nguyen et al., Design of a neutron flux measurement channel using the ionization chamber KNK-3 at the Dalat Nuclear Research Reactor. J. Nuclear Sci. Technol. **11**, 11–18 (2021). https://doi.org/10.53747/nst.v11i3.367
12. Y.L. Zhou, S.L. Qiu, M.T. Ge et al., Analysis of reliability and life of fission ionization chamber of Nuclear Instrumentation System (NIS). Int. Conf. Nuclear Eng. ASME (2022). https://doi.org/10.1115/ICONE29-92683
13. Spectrometers Accelerators, S. Chabod, G. Fioni, A. Letourneau et al., Modelling of fission chambers in current mode-analytical approach. J. Nuclear Instruments and Methods in Physics Research Section A. Detectors and Associated Equipment **566**, 633–653 (2006). https://doi.org/10.1016/j.nima.2006.06.067
14. S.K. Mohanan, H. Boukabache, V. Cruchet et al., An ultra low current measurement mixed-signal ASIC for radiation monitoring using ionisation chambers. J. IEEE Sensors J. **22**, 2142–2150 (2022). https://doi.org/10.1109/JSEN.2021.3132498
15. Y. Huang, M. Zhou, A. Yu et al., Noise suppression for weak current measurement based on neural-network-assisted UHV FOCS. J. Opt. Laser Technol. **151**, 107995 (2022). https://doi.org/10.1016/j.optlastec.2022.107995
16. C. Krause, D. Drung, H. Scherer, Measurement of sub-picoampere direct currents with uncertainties below ten attoamperes. J. Rev. Sci. Instrum. **88**, 024711 (2017). https://doi.org/10.1063/1.4975826
17. C.Y. Zhou, H. Su, R.S. Mao et al., An accurate low current measurement circuit for heavy iron beam current monitor. J. Nucl Instrum Methods Phys Res Sect B **280**, 84–87 (2012). https://doi.org/10.1016/j.nimb.2012.01.033
18. N. Ni, X.F. Xiao, L.Q. Ge et al., The research on IV convertor for low-level current measurement. J. Nucl. Electron. Detect. Technol. **33**, 665–669 (2013). https://doi.org/10.3969/j.issn.0258-0934.2013.06.003
19. R.J. Zhu, X. Zhou, Z.H. Liu et al., High-precision and wide-range real-time neutron flux monitor system through multipoint linear calibration. Nucl. Sci. Tech. **31**, 94 (2020). https://doi.org/10.1007/s41365-020-00798-3
20. V. Shenoy, S. Jung, Y. Yoon et al., A CMOS analog correlator-based painless nonenzymatic glucose sensor readout circuit. J. IEEE Sens J. **14**, 1591–1599 (2014). https://doi.org/10.1109/JSEN.2014.2300475
21. D. Wen, X. Liang, M. Su et al., Error correction of weak current measurement system based on wavelet denoising and generalized regression neural network. Inst. Mesure Métrologie **20**, 91–99 (2021). https://doi.org/10.18280/i2m.200205
22. X.P. Yu, X.G. Tuo, D.S. Xi et al., Current measurement of wide range fA level in ionization chamber. J. Nucl. Electron. Detect. Technol. **31**, 1181–1185 (2011). https://doi.org/10.3969/j.issn.0258-0934.2011.10.027
23. A.M. Abdul, M.F. Pervez, M.K. Hossain et al., Pico-current measurement challenges and remedies: A review. J. Univers. J. Eng. Sci. **5**, 57–63 (2017). https://doi.org/10.13189/ujes.2017.050401
24. S.L. Hao, D.S. Xi, X.G. Tuo et al., Design of ionization chamber current measuring instrument based on DDC112. J. Nucl. Electron. Detect. Technol. **32**(1309–1313), 1335 (2012). https://doi.org/10.3969/j.issn.0258-0934.2012.11.019
25. W. Wang, M. Cui, M.W. Li et al., Design of pA level current signal detection circuit. J. North Univ. China. Nat. Sci. Ed. **40**, 173–179 (2019). https://doi.org/10.3969/j.issn.1673-3193.2019.02.014
26. Z.C. Guo, G.F. Liu, S.L. Wu et al., Research on design of weak current measurement system based on IV convertor. 2017 2nd

International Conference on MSMEE. 812-817 (2017). https://doi.org/10.2991/msmee-17.2017.159
27. R.G. Ma, B.Q. Cui, Y.J. Ma et al., Weak current measurement system in BRISOL. Nucl. Tech. (in Chinese) **37**, 080402 (2014). https://doi.org/10.11889/j.0253-3219.2014.hjs.37.080402
28. D. Kim, B. Goldstein, W. Tang et al., Noise analysis and performance comparison of low current measurement systems for biomedical applications. J. IEEE Trans. Biomed .Circ. Syst. **7**, 52–62 (2012). https://doi.org/10.1109/TBCAS.2012.2192273
29. C.F. Dong, H. Su, J.P. Xing et al., The I-F converter in the weak current measurement. J. Nucl. Electron. Detect. Technol. **24**, 488–489 (2004). https://doi.org/10.3969/j.issn.0258-0934.2004.05.013
30. G.R. Wang, The I-F converter design for very weak current measurement. J. Nucl. Electron. Detect. Technol. **25**, 358–362 (2005). https://doi.org/10.3969/j.issn.0258-0934.2005.04.005
31. L.Q. Wei, S.J. Lei, M.H. Fang et al., An IV converter in picoampere current measurement. J. Inst. Anal. Monitor. **3**, 28–31 (2010). https://doi.org/10.3969/j.issn.1002-3720.2010.03.010
32. S.L. Hao, X.G. Tuo, H.H. Wang et al., Design of weak current measurement with capacitor-integration based on STM32. J. Electr. Meas. Instrum. **8**, 84–88 (2012). https://doi.org/10.3969/j.issn.1001-1390.2012.08.019
33. G.Y. Zhang, X.G. Tuo, H.H. Wang et al., Comparison and improvement with the capacity of C/R measurement method of fA level current. J. Electr. Meas. Instrum. **12**, 8–12 (2011). https://doi.org/10.3969/j.issn.1001-1390.2011.12.003
34. X. Zhao, N. NI, Q.X. Zhang et al., A current to frequency conversion based circuit for low-level current measurement. Nucl. Tech. (in Chinese) **45**, 41–46 (2022). https://doi.org/10.11889/j.0253-3219.2022.hjs.45.020401
35. R.E. Kalman, A new approach to linear filtering and prediction problems. J. Basic Eng. Mar. **82**, 35–45 (1960). https://doi.org/10.1115/1.3662552
36. R.I. Alfian, A. Ma'arif, S. Sunardi, Noise reduction in the accelerometer and gyroscope sensor with the Kalman filter algorithm. J. JRC. **2**, 180–189 (2021). https://doi.org/10.18196/jrc.2375
37. B. Ehtesham, T. John, Automation for calibrating a precision current source by Ohm's law method. J. IJPAP. **58**, 99–105 (2020)
38. H.M. Parsons, D.R. Ekman, T.W. Collette et al., Spectral relative standard deviation: a practical benchmark in metabolomics. J. Analyst. **134**, 478–485 (2009)
39. X.F. Lu, M. Peng, Y.Y. Yuan et al., Determination of 21 mineral elements in two species of comastoma by ICP-OES. J. Nat. Prod. Res. Dev. **27**, 837 (2015). https://doi.org/10.16333/j.1001-6880.2015.05.016

Springer Nature or its licensor (e.g. a society or other partner) holds exclusive rights to this article under a publishing agreement with the author(s) or other rightsholder(s); author self-archiving of the accepted manuscript version of this article is solely governed by the terms of such publishing agreement and applicable law.